ARTICLE

Extracellular Vesicle ITGAM and ITGB2 Mediate Severe Acute Pancreatitis-Related Acute Lung Injury

Qian Hu, Shu Zhang, Yue Yang, Juan Li, Hongxin Kang, Wenfu Tang, Christopher J. Lyon, and Meihua Wan*

Read Online

ACCESS | Metrics & More | Article Recommendations | Supporting Information

ABSTRACT: Integrins expressed on extracellular vesicles (EVs) secreted by various cancers are reported to mediate the organotropism of these EVs. Our previous experiment found that pancreatic tissue of mice with severe cases of acute pancreatitis (SAP) overexpresses several integrins and that serum EVs of these mice (SAP-EVs) can mediate acute lung injury (ALI). It is unclear if SAP-EV express integrins that can promote their accumulation in the lung to promote ALI. Here, we report that SAP-EV overexpress several integrins and that preincubation of SAP-EV with the integrin antagonist peptide HYD-1 markedly attenuates their pulmonary inflammation and disrupt the pulmonary microvascular endothelial cell (PMVEC) barrier. Further, we report that injecting SAP mice with EVs engineered to overexpress two of these integrins (ITGAM and ITGB2) can attenuate the pulmonary accumulation of pancreas-derived EVs and similarly decrease pulmonary inflammation and disruption of the endothelial cell barrier. Based on these findings, we propose that pancreatic EVs can mediate ALI in SAP patients and that this injury response could be attenuated by administering EVs that overexpress ITGAM and/or ITGB2, which is worthy of further study due to the lack of effective therapies for SAP-induced ALI.
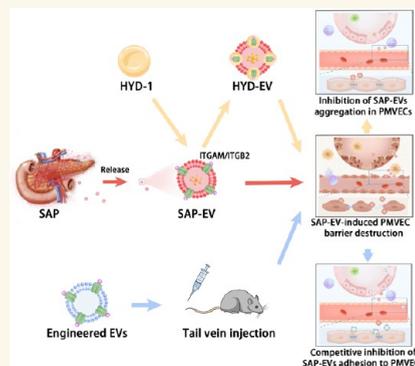
KEYWORDS: *extracellular vesicles, severe acute pancreatitis, acute lung injury, integrin α M, integrin β 2, pulmonary microvascular endothelial cells*

INTRODUCTION

Acute pancreatitis (AP) is an inflammatory disorder of the exocrine pancreas, which often causes local pancreatic or extrapancreatic organ inflammation and injury,[1] and its severity can be divided into mild, moderately severe, and severe cases.[2] Mild AP (MAP) does not produce organ failure or local or systematic complications and often resolves spontaneously within days, but severe AP (SAP) can produce persistent systemic inflammatory response syndrome (SIRS)-associated organ failure (single or multiple, after >48h).[3,1] Acute lung injury (ALI) is one of the most serious complications of SAP, and clinical data show that SAP patients with ALI have higher incidence of renal failure, cardiovascular failure, and higher mortality.[4] Early mortality (within 1 week of onset) in SAP patients with ALI is as high as 70%,[5] and thus, it is very important to prevent or treat ALI to reduce SAP-associated mortality. Pathogen-derived toxins, microcirculation disturbances, pro-inflammatory immune cell activation, and cytokine dysregulation are all considered potential mechanisms that may underlie the development of SAP-ALI.[6,7] And, mesenteric

lymphatic circulation is considered the primary route through which these factors enter lung tissue, and that interruption of mesenteric lymphatic flow can prevent ALI in AP rats before the development of ALI, but the same results cannot be obtained clinically due to the complexity of human function.[6,8] Current clinical treatment of SAP-ALI is therefore still limited to fluid management and supportive care.[9] Exploring the exact pathophysiological mechanisms of SAP-ALI remains a top priority, and the development of drugs for the prevention/ treatment of SAP-ALI based on these mechanisms would lead to important changes in SAP outcomes.

The alveolar-capillary barrier, composed of pulmonary epithelial cells, alveolar macrophages, pulmonary microvascular
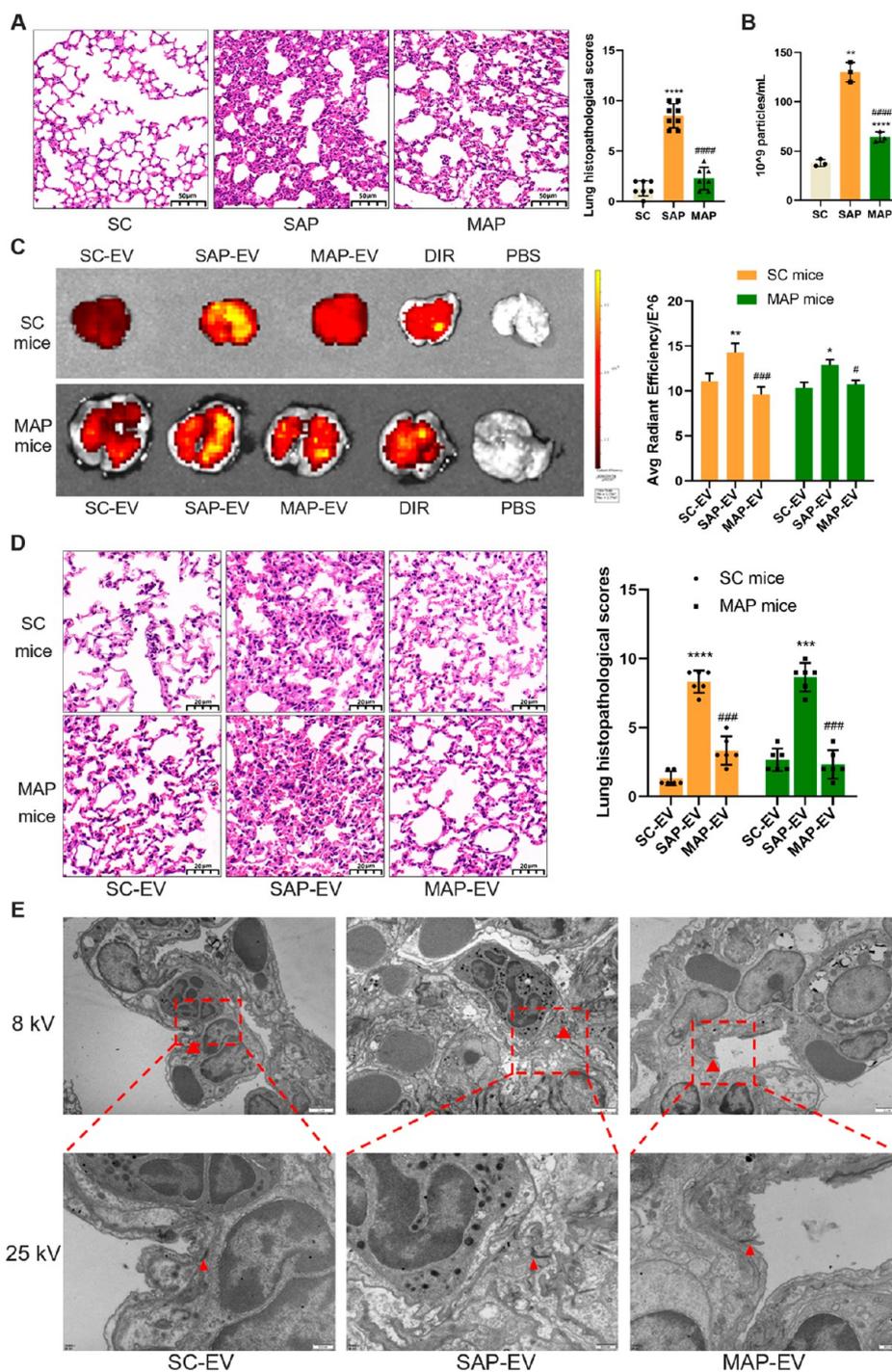
Figure 1. SAP-EV administration disrupts PMVEC connections to promote ALI. (A) Representative lung histology and pathology scores for lung tissue of mice belonging to the sham control (SC) and mild and acute pancreatitis (MAP and SAP) groups ($n = 6$/group; scale bar = 50 μm, ****$p < 0.0001$ vs SC, ####$p < 0.0001$ vs SAP). (B) Serum EV concentrations for the SC, MAP and SAP groups ($n = 3$/group; **$p < 0.01$ vs SC, ****$p < 0.0001$ vs SC, ####$p < 0.0001$ vs SAP). (C) Representative fluorescence images and statistical analysis of SC and MAP mouse lung tissue after tail-vein injection with SC-, MAP-, and SAP-EV, an equal amount of free DIR, or an equal volume of PBS ($n = 3$/group; *$p < 0.05$, **$p < 0.01$ vs SC-EV, #$p < 0.05$, ###$p < 0.001$ vs SAP-EV). (D) Representative lung histology and pathology scores of sham and MAP mice after SC-, MAP-, and SAP-EV injection ($n = 6$/group, scale bar = 20 μm, ***$p < 0.001$, ****$p < 0.0001$ vs SC-EV, ###$p < 0.001$ vs SAP-EV). (E) Electron microscopic images of tight junctions between PMVECs in SC mice after the indicated EV injections. Red arrows indicate tight junction connections between PMVECs (scale bar = 2 μm in 8kv, scale bar = 500 nm in 25kv).

endothelial cells (PMVECs), and fibroblasts, maintains the homeostasis of lung tissue.[10] Damage to this barrier that results in increased alveolar permeability is a key characteristic of ALI, as this allows water, red blood cells, pro-inflammatory factors (*e.g.*, reactive oxygen species [ROS] and tumor necrosis factor-

α [TNFα]), and immune cells (*e.g.*, neutrophils and monocytes) to freely enter and exit the alveoli, which promotes lung inflammation and dysfunction.[7,8,11] PMVECs that line vessels of the pulmonary circulatory system maintain their integrity and act as highly impermeable barriers that prevent
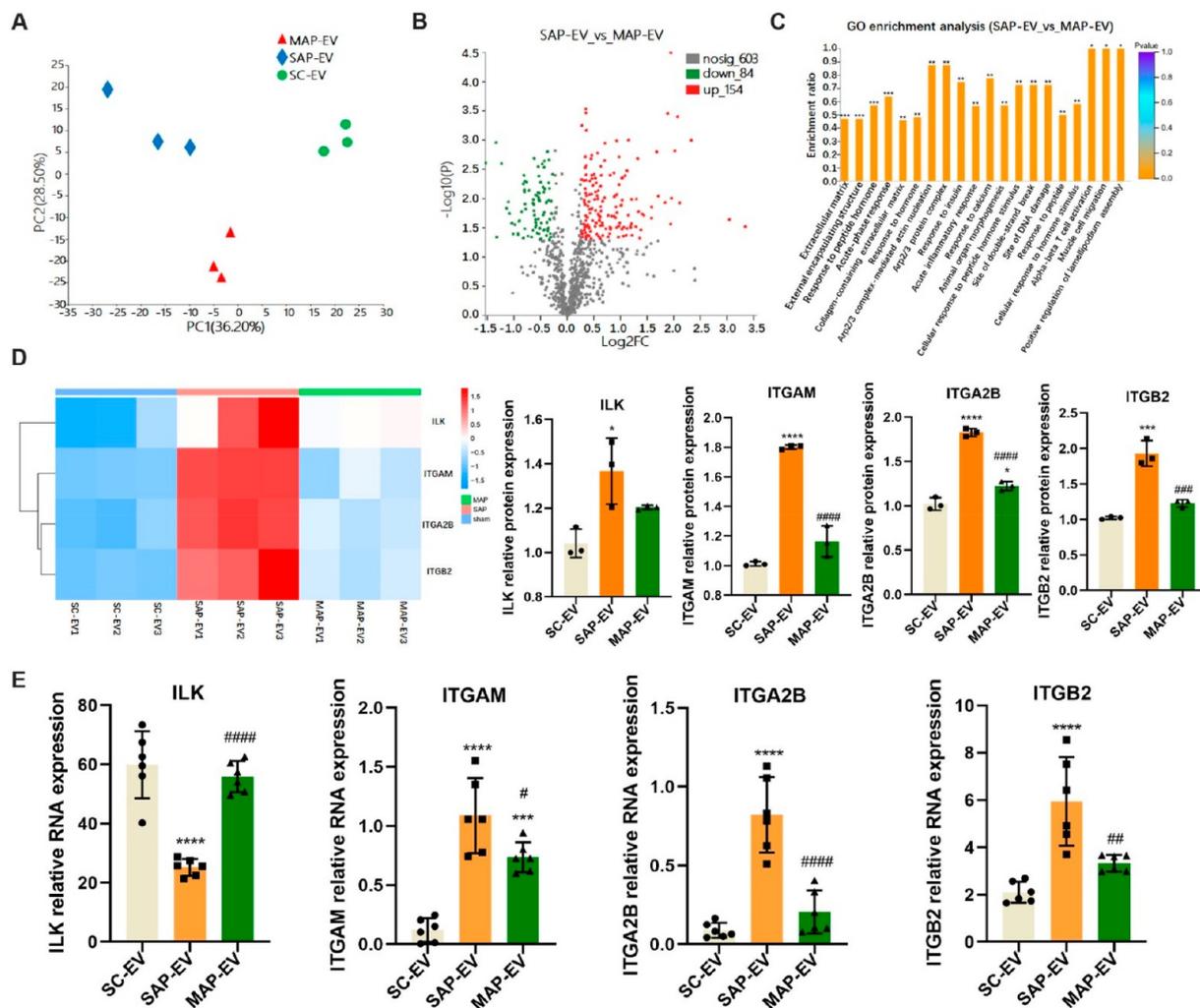
Figure 2. SAP-EV abundantly express ITGAM and ITGB2. Extracellular vesicles were extracted from the serum of the three groups mice and analyzed by proteomics. (A) Principal component analysis (PCA) of three groups of EVs (SC-EV, MAP-EV, and SAP-EV) proteomics. (B) Volcano diagram of protein expression differences between SAP-EV and MAP-EV group. (C) GO enrichment analysis of protein expression differences between SAP-EV and MAP-EV group (*$p < 0.05$, **$p < 0.01$, ***$p < 0.001$). (D) Heat map and statistical analyses of integrin protein expression in three groups EVs ($n = 3$/group; *$p < 0.05$, ***$p < 0.001$, ****$p < 0.0001$ vs SC-EV, ###$p < 0.001$, ####$p < 0.0001$ vs SAP-EV). (E) qPCR was used to detect the mRNA levels of integrin-related proteins ILK, ITGA2B, ITGAM, and ITGB2 in the three groups of EVs ($n = 6$/group; ***$p < 0.001$, ****$p < 0.0001$ vs SC-EV, #$p < 0.05$, ##$p < 0.01$, ####$p < 0.0001$ vs SAP-EV).

the free passage of water, solutes, pathogens, and immune cells between the microvessels and the lung interstitium.[11,12] PMVEC dysfunction (*e.g.*, abnormal proliferation, apoptosis, necrosis, or tight junction disruption) can disrupt this barrier and promote the development of ALI.[11,13] Restoring PMVEC barrier integrity or preventing its disruption is thus a good means to treat ALI caused by dysregulation of endogenous cytokines (*e.g.*, TNFα and IL-6).[14] For example, inhibiting ROS production in mouse lung tissue can upregulate endothelial cell expression of the tight junction proteins zonulaoccludens-1 (ZO-1) and occludin to maintain the function of the alveolar-capillary endothelial barrier and ultimately attenuate sepsis-induced ALI.[15]

Extracellular vesicles (EVs) are small vesicles that can transfer a variety of bioactive substances (proteins, nucleic acids, lipids, *etc.*) to adjacent and distant cells and tissues to regulate disease development and progression as well as physiologic processes.[16] We have previously reported that EVs produced during SAP (SAP-EVs) accumulate in lung tissue after peripheral injection and can participate in the ALI

development by inducing pro-inflammatory polarization of alveolar macrophages and the secretion of inflammatory factors.[4] However, PMVECs are the earliest cells damaged in SAP-ALI,[17] and it is not clear if SAP-EV directly act on PMVECs to mediate SAP-ALI.

EV surface molecules can promote their selective uptake by specific tissues. For example, tumor-derived EVs that express integrins α6β4 and α6β1 can promote lung metastasis, and primarily colocalize with S100 calcium binding protein A4 (S100A4)-positive fibroblasts and surfactant protein C (SPC)-positive epithelial cells in the lung.[18] We therefore analyzed EVs isolated from mouse models of MAP and SAP to identify EV surface proteins that could explain the SAP-EV lung accumulation phenotype and detected the enrichment of multiple integrins. Since integrins regulate PMVEC cytoskeleton structure, barrier function, angiogenesis, and inflammatory responses,[19,20] we hypothesized that altered integrin expression on SAP-EV might permit these EVs to target PMVECs during SAP events to promote ALI.
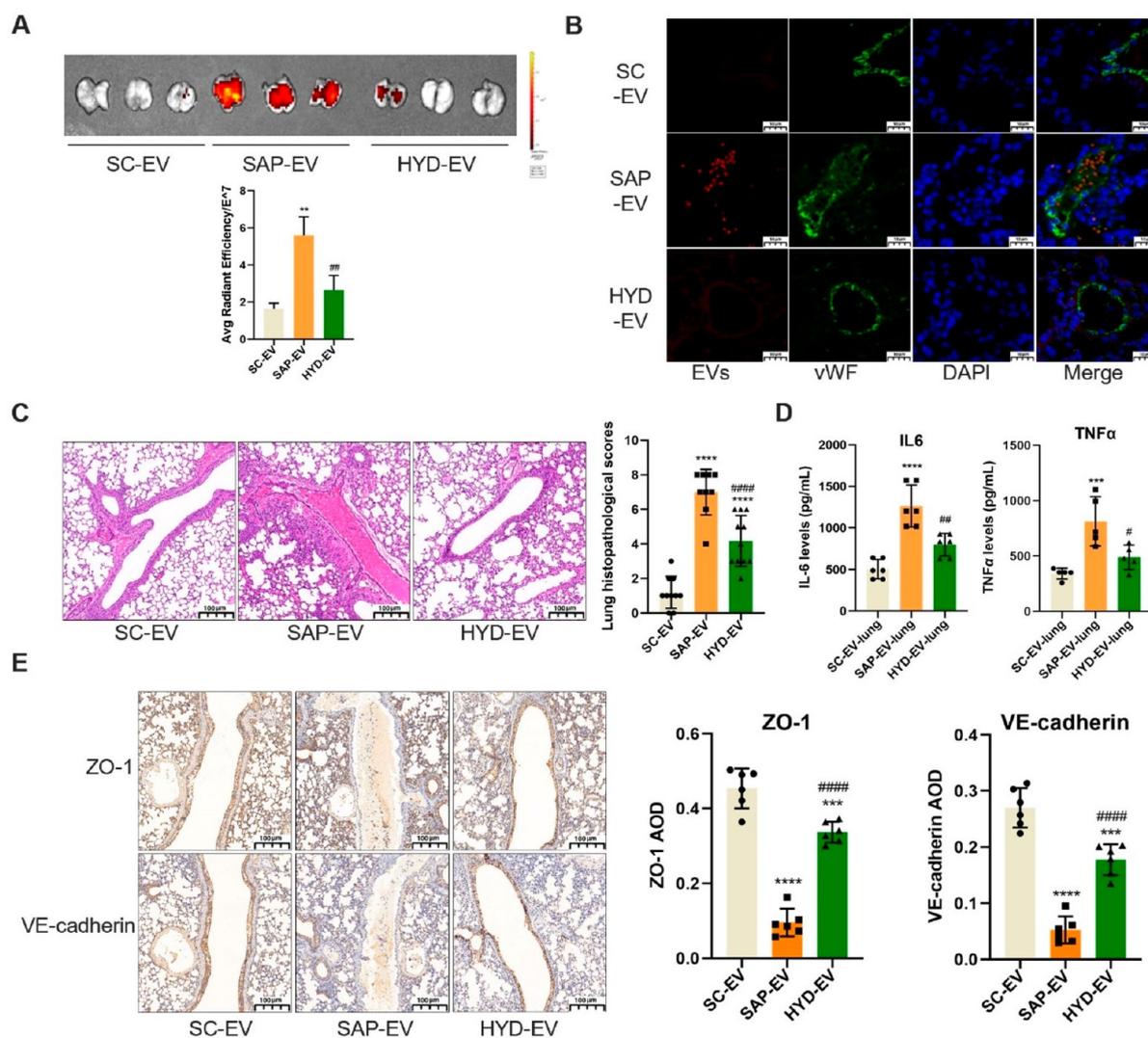
Figure 3. HYD-1-inhibition reduces SAP-EV-induced lung injury responses. (A) DIR signal in lungs of healthy mice after tail-vein injection with DIR-labeled SAP-EV, SAP-EV preincubated with HYD-1 (HYD-EV), or SC-EV fractions (n = 3/group; **$p < 0.01$ vs SC-EV, ##$p < 0.01$ vs SAP-EV). (B) Representative histology of EV colocalization with lung tissue microvascular endothelial cells (vWF positive) after EV injection (scale bar = 10 μm). (C) Lung histology and pathology scores of healthy mice after EV injection (n = 10/group; scale bar = 100 μm, ****$p < 0.0001$ vs SC-EV, ####$p < 0.0001$ vs SAP-EV). (D) Lung IL-6 and TNFα expression after EV injection (n = 6/group; ***$p < 0.001$, ****$p < 0.0001$ vs SC-EV-lung, #$p < 0.05$, ##$p < 0.01$ vs SAP-EV-lung). (E) Lung immunohistology and graphs of VE-cadherin and ZO-1 expression after EV injection (n = 6/group; ***$p < 0.001$, ****$p < 0.0001$ vs SC-EV, ####$p < 0.0001$ vs SAP-EV).

Studies were performed to address this question, which indicated that healthy mice injected with SAP-EV developed lung tissue injury and inflammation responses consistent with ALI and that pulmonary SAP-EV accumulation occurred in an integrin-dependent manner that could be attenuated by preincubating SAP-EV with the integrin antagonist peptide HYD-1 or by injection with EVs engineered to overexpress ITGAM or ITG2B, both of which are overexpressed on SAP-EV. These findings suggest that administering EVs or other particles engineered to highly express these integrins could attenuate lung SAP-EV accumulation to improve the poor prognosis of SAP-ALI.

RESULTS AND DISCUSSION

SAP-EV Administration Disrupts PMVEC Connections to Promote ALI. Mice were given intraperitoneal injections of caerulein and retrograde injections of taurocholic acid sodium salt hydrate *via* the pancreatic duct to, respectively, establish mouse models of MAP and SAP used to explore mechanism of SAP-ALI.[21] SAP mice demonstrated progressive lung injury phenotypes (alveolar wall thickening, hemorrhage, inflammatory cell infiltration) when compared to the sham control (SC) and MAP groups (Figure 1A), and these changes were accompanied by progressive serum EV increases (Figure 1B). To explore whether these serum EV increases can induce the development of SAP-ALI, equal amounts of serum EVs isolated from SC, MAP, and SAP mice (SC-EV, SAP-EV, and MAP-EV) were labeled with the lipophilic fluorescent dye DIR and injected into the tail veins of SC or MAP mice. These samples exhibited similar labeling, but DIR signal was significantly higher in the lungs of SC mice injected with SAP-EVs versus SC-EVs or MAP-EVs, which did not differ with and injected MAP mice yielded similar results (Figure 1C). SAP-EV-injected SC and MAP mice revealed similar lung histology and pathology scores, which were greater than those observed after injection with SC-EVs or MAP-EVs (Figure
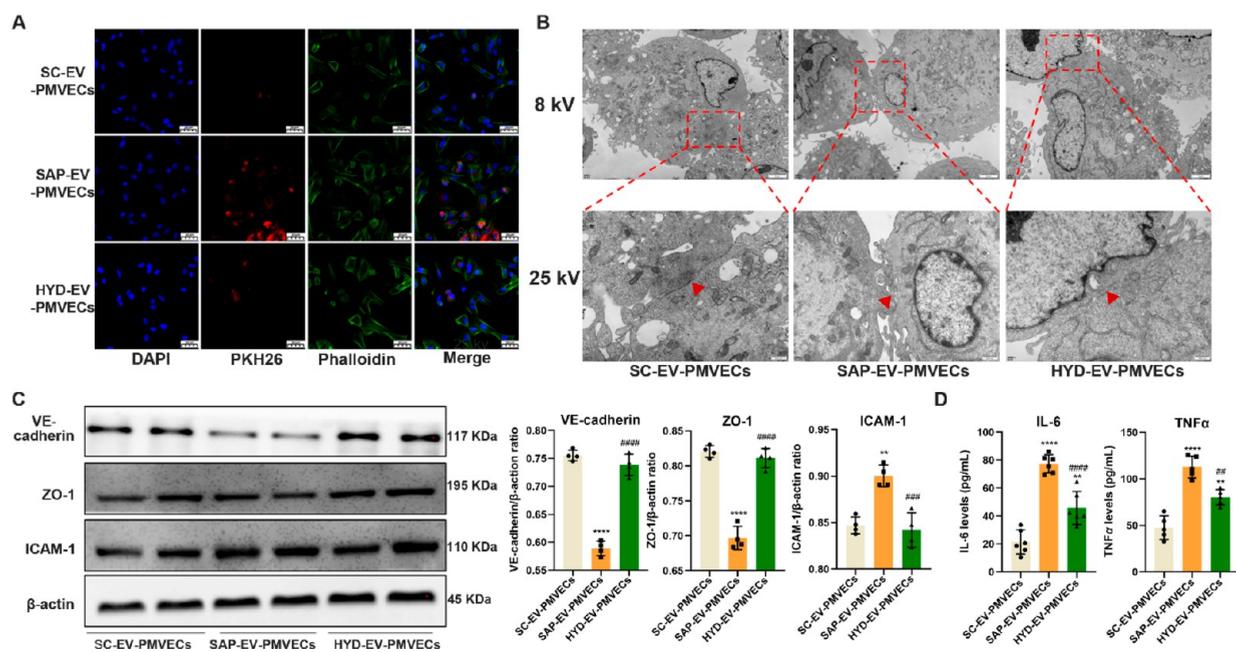
Figure 4. SAP-EV integrin attenuates PMVEC tight junction proteins expression. (A) Representative histology of SC-EV, SAP-EV, and HYD-EV colocalization with cultured PMVECs (scale bar = 20 μm). (B) Electron microscopy images of PMVECs cell tight junctions (red arrow) after SC-EV, SAP-EV, and HYD-EV incubation (8 kV scale bar = 2 μm, 25 kV scale bar = 500 nm). (C) Western blot analysis and graphs of PMVEC VE-cadherin, ZO-1, and ICAM-1 expression after EV incubation (n = 4/group; **p < 0.01, ****p < 0.0001 vs SC-EV-PMVECs, ###p < 0.001, ####p < 0.0001 vs SAP-EV-PMVECs). (D) IL-6 and TNFα expression in PMVEC culture supernatant after EV incubation (n = 6/group; **p < 0.01, ****p < 0.0001 vs SC-EV-PMVECs, ##p < 0.01, ####p < 0.0001 vs SAP-EV-PMVECs).

1D). DIR signal detected in the lungs of SAP-EV-injected SC mice was associated with pulmonary microvascular endothelial cells (vWF-positive) and alveolar macrophages (CD68-positive) but not epithelial cells (SPC-positive) and fibroblasts (S100A4-positive) (Figure S1). SC mice injected with SAP-EV, but not SC-EV and MAP-EV, had PMVEC tight junction disruptions, indicated by tiny cracks in this structure in lung tissue electron micrographs (Figure 1E). These studies indicate that SAP mice have greater lung pathology and higher serum EV levels than MAP mice; that SAP-EVs exhibit greater pulmonary accumulation than MAP-EVs after injection; and that SAP-EVs induce lung phenotypes consistent with SAP-ALI, suggesting that SAP-EVs preferentially target lung tissue and carry factors that promote SAP-associated pulmonary injury responses.

SAP-EV Abundantly Express ITGAM and ITGB2. Since interactions between EV and cell surface proteins have previously been shown to promote organotropism,[18,22,23] we employed proteomics to explore potential differences in proteins expressed by SC-EVs, MAP-EVs, and SAP-EVs. Principal component analysis (PCA) detected consistent differences between these three groups (Figure 2A), and the MAP-EV and SAP-EV proteomes revealed significant differential expression for 238 proteins (84 decreased, 154 increased) (Figure 2B). GO enrichment analysis found these 238 proteins were primarily associated with the extracellular matrix, peptide hormone responses, and acute-phase responses (Figure 2C). RNA sequence analysis detected 27 integrin transcripts that were upregulated in pancreatic tissue of SAP versus SC and MAP mice (Figure S2). Extraction of integrin-related protein expression from our proteomics data found that integrin α-M (ITGAM), α-2B (ITGA2B), and β-2 (ITGB2) were overexpressed in SAP-EV versus SC-EV and MAP-EV samples, but integrin-liked kinase (ILK) expression did not

significantly differ between the SAP-EV and MAP-EV samples (Figure 2D). RT-qPCR analysis detected a trend toward increased ITGAM, ITGA2B, and ITGB2 mRNA expression from the SC-EV to the MAP-EV and SAP-EV samples (Figure 2E) corresponding with the expression patterns of their protein products. However, ILK mRNA levels were discordant with ILK protein expression in these EVs, which could reflect the activity posttranscriptional or posttranslational mechanisms that regulate ILK expression,[24] including differential regulation of ubiquitination events reported to mediate its degradation.[25] This discordance could potentially also reflect differential sorting of ILK protein and mRNA into pancreatic EVs in these mice if a SAP-mediated process affects these pathways.

HYD-1-Incubation Inhibits SAP-EV-Induced Lung Injury. To explore whether SAP-EV integrin regulates SAP-mediated pulmonary inflammation, we synthesized the D-amino acid integrin targeting peptide HYD-1 (KIKMVI-SWKG) and incubated SAP-EV with this peptide to generate an EV fraction where integrin binding was blocked by HYD1 binding (HYD-EV).[26,27] Healthy mice were then injected with equal SC-EV, SAP-EV, or HYD-EV doses to examine the integrin-dependence of SAP-EV-mediated lung injury. Mice injected with SAP-EVs revealed increased lung accumulation and uptake by lung endothelial cells and greater evidence of PMVEC tissue injury (hemorrhage and inflammatory cell infiltration) than mice injected with SC-EVs, while mice injected with HYD-EVs revealed reductions in all these SAP-EV-induced lung phenotypes (Figure 3A−C), suggesting that SAP-EV integrin mediates all these effects. Mice injected with SAP-EVs also revealed an increase in pulmonary IL-6 and TNFα expression that was attenuated in mice injected with HYD-EVs (Figure 3D). Since SAP-EV can cause red blood cells and inflammatory cell to invade the pulmonary microvascular cavity, we examined the expressions of two major tight
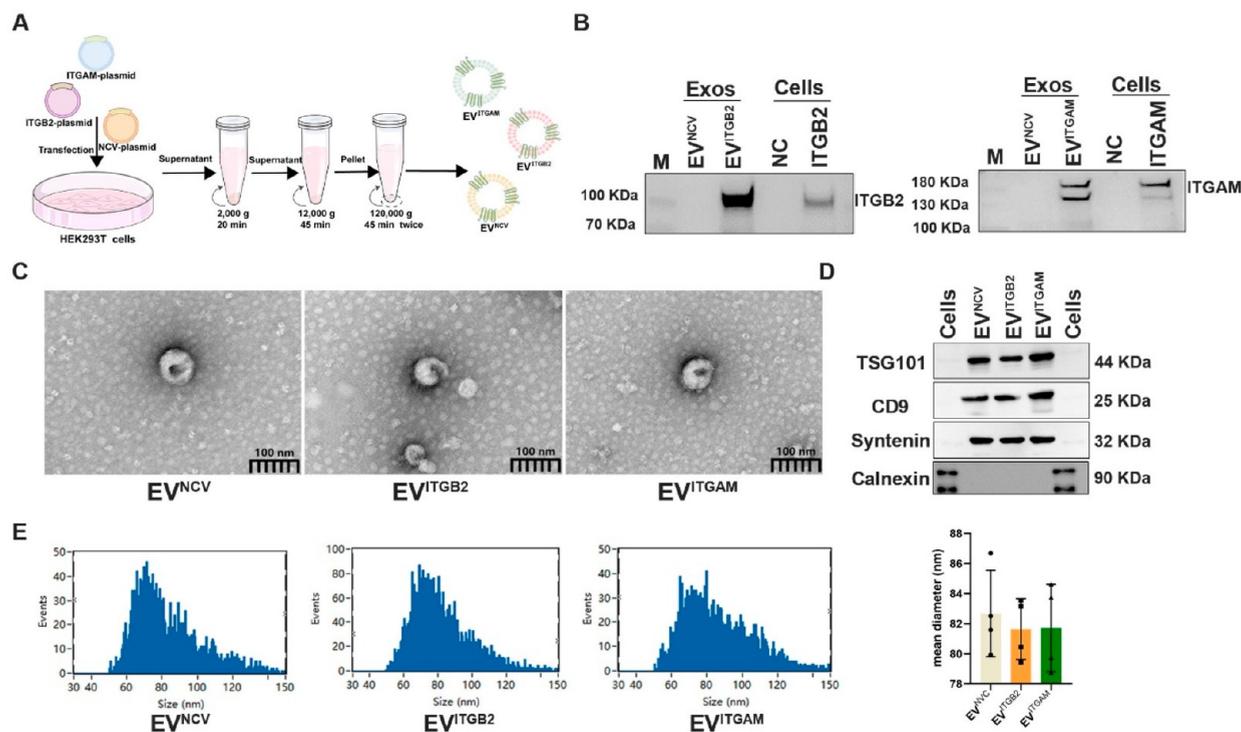
Figure 5. Generation of ITGAM/ITGB2 overexpressing EVs. (A) HEK293T cells transfected with ITGB2, ITGAM, or empty expression vectors to isolate EVs overexpressing ITGB2 (EV^ITGB2) or ITGAM (EV^ITGAM) or negative control EVs (EV^NCV) by ultracentrifugation of culture supernatants. **(B)** Western blot analysis of ITGB2 and ITGAM expression in transfected cells and their EV isolates. **(C)** Transmission electron micrographs of EV fractions. **(D)** Western blot analysis of positive (TSG101, CD9, and Syntenin) and negative (calnexin) EV marker proteins. **(E)** Size distribution and mean diameter of EV fractions determined by nanoparticle tracking analysis (bar chart: n = 3/group).

junction proteins [vascular endothelial cell cadherin (VE-cadherin) and ZO-1, which maintain endothelial function][28] in lung endothelial cells of mice injected with SC-EVs, SAP-EVs, or HYD-EVs. Healthy mice injected with SAP-EVs expressed markedly less endothelial VE-cadherin and ZO-1 protein than SC-EV-injected mice, while mice injected with HYD-EVs revealed a strong attenuation of the protein losses detected in the SAP-EV-treated mice (Figure 3E). These results indicate that SAP-EVs injected into healthy mice can induce lung injury and inflammation phenotypes consistent with those detected in SAP mice. This suggests that SAP-EV factors are sufficient to induce these responses; that SAP-EV integrins play a critical role in their pulmonary accumulation; and that disruption of the pulmonary endothelial barrier in this process is due to SAP-EV effects to dysregulated VE-cadherin and ZO-1 expression.

SAP-EV Integrin Attenuates the Expression of Tight Junction Proteins on PMVECs. To confirm that SAP-EVs directly interact with PMVECs, we incubated isolated mouse PMVECs with SC-EV, SAP-EV, and HYD-EV samples fluorescently labeled with PKH26. There was a clear difference in EV uptake among these groups (SAP-EV > HYD-EV > SC-EV), suggesting that integrin expression is required for efficient SAP-EV uptake (Figure 4A). PMVECs incubated with SAP-EVs revealed disruptions in their tight junctions that were reduced or absent in cells incubated with HYD-EVs, suggesting this effect was also integrin dependent (Figure 4B). SAP-EV treatment, but not HYD-EV treatment, also decreased VE-cadherin and ZO-1 and increased intercellular adhesion molecule 1 (ICAM-1) protein expression in these cells (Figure 4C). Notably, reduced VE-cadherin and ZO-1 expression

detected in the SAP-EV-treated cells was consistent with reduced endothelial interaction and barrier disruption, while increased ICAM-1 expression was consistent with PMVEC injury as it is an important marker of acute lung injury, enhances the leukocyte adhesion and activation, and induces a "cascade" of inflammatory mediators and pulmonary microcirculation dysfunction.[29] SAP-EV treatment also markedly increased PMVEC secretion of IL-6 and TNFα, which was attenuated when these cells were incubated with HYD-EV (Figure 4D). SAP-EVs thus produce similar pathologic effects on lung PMVECs *in vivo* and *in vitro*, strongly implying that SAP-EVs may be sufficient to mediate their phenotype in the absence of regulatory processes mediated by other systemic factors.

Generation of ITGAM/ITGB2 Overexpressing EVs. SAP-EVs overexpress ITGAM and ITGB2 that heterodimerize to form integrin αmβ2 [also known as macrophage-1 antigen (Mac-1)], which is implicated in intercellular migration and adhesion processes,[30−32] but ITGA2B is related to coagulation response.[33,34] Thus, to individually evaluate the effect of ITGAM and ITGB2 on lung injury, we transfected human embryonic kidney 293T (HEK293T) cells with ITGAM or ITGB2 expression vectors or an empty expression cassette (negative control vector, NCV) (Figure 5A) to produce EVs that specifically overexpress one of these two integrins (EV^ITGAM or EV^ITGB2) or exhibit normal integrin expression (EV^NCV). Western blot analysis confirmed ITGAM or ITGB2 overexpression in the corresponding recombinant HEK293T cells and EV isolates versus cells transfected with negative control vector and their EVs (Figure 5B). EV fractions of these cells were of the expected size and morphology and were
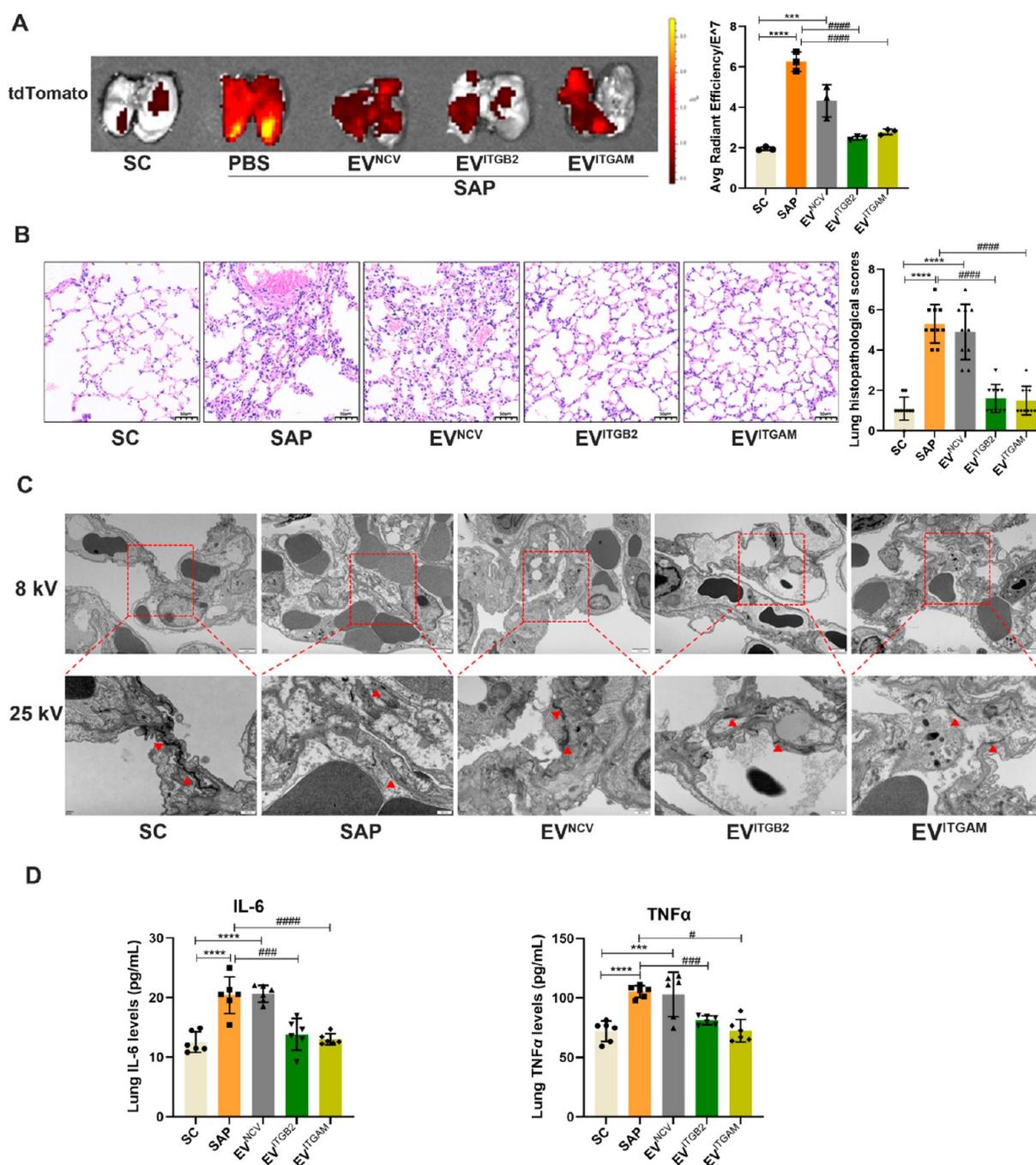
Figure 6. EV^{ITGB2} and EV^{ITGAM} treatment blocks lung EV accumulation and inflammation in SAP mice. Pdx1-cre mice were selected to establish SAP model, and then, three groups of engineered EVs (EV^{ITGB2}, EV^{ITGAM}, and EV^{NCV}) labeled with PKH67 fluorescent dye were injected into pdx1-cre-SAP mice by tail vein. (A) Representative images and graph of pancreatic EV accumulation (tdTomato fluorescence) in the lungs of transgenic SAP mice ($n = 3$/group; ***$p < 0.001$, ****$p < 0.0001$ vs SC, ####$p < 0.0001$ vs SAP). (B) Representative lung histology and pathology scores of SC, SAP, and EV-treated SAP mice ($n = 10$; scale bar = 50 μm, ****$p < 0.0001$ vs SC, ####$p < 0.0001$ vs SAP). (C) Transmission electron microscopy images of tight junctions between lung endothelial cells of lung tissue of SC, SAP, and EV-treated SAP mice (8 kV scale bar = 2 μm, 25 kV scale bar = 500 nm). (D) ELISA data for the IL-6 and TNFα concentrations in lung tissue of each group ($n = 6$/group; ***$p < 0.001$, ****$p < 0.0001$ vs SC, #$p < 0.05$, ###$p < 0.001$, ####$p < 0.0001$ vs SAP).

enriched for three EV-associated protein markers (TSG101, CD9, and Syntenin) but not an endoplasmic reticulum-associated protein (calnexin) employed as an indicator or cytoplasmic contamination (Figure 5C,D). Mean particle diameters in these EV samples ranged from 79 to 86 nm, with most particles falling within the expected range for exosomes (30−150 nm) (Figure 5E).

EV^{ITGB2} and EV^{ITGAM} Treatment Reduces Pancreatic EV Accumulation and Inflammation in the Lungs of a Mouse SAP Model. We next established a transgenic mouse model where pancreas-specific pdx-cre expression activated red fluorescent tdTomato expression in pancreas-derived EVs to allow for their sensitive and specific detection.[35] Subsequent analysis of pdx1 protein expression and red fluorescent signal in serum EVs of SC, SAP, and MAP transgenic mice detected a
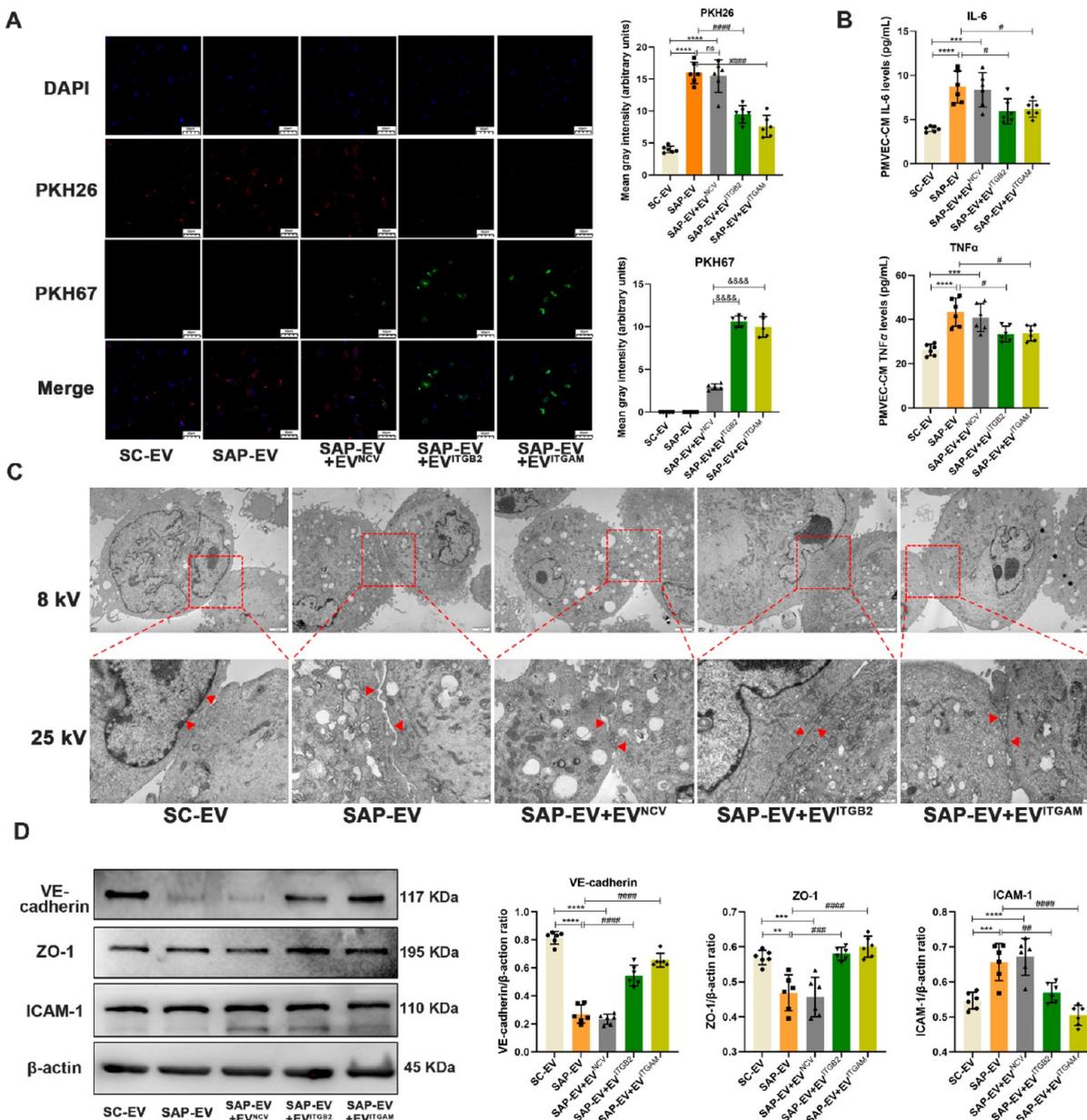
Figure 7. EV^{ITGB2} and EV^{ITGAM} inhibit SAP-EV-mediated effects to induce PMVEC tight junction disruption and inflammation. Serum EVs of sham control group and SAP group mice (SC-EV and SAP-EV) were labeled with PKH26 fluorescence, and exogenous engineered EVs (EV^{ITGB2}, EV^{ITGAM}, and EV^{NCV}) were labeled with PKH67 fluorescence. Then, two kinds of EVs were used to interfere with primary pulmonary vascular endothelial cells (PMVECs) of mice. (A) Representative images and quantitation of PMVEC uptake of PKH26-stained SC-EV and SAP-EV fractions (red) and PKH67-stained EV^{ITGB2}, EV^{ITGAM}, and EV^{NCV} fractions (green) by DAPI-stained (blue) PMVECs (n = 6/group; ****$p < 0.0001$ vs SC-EV, ####$p < 0.0001$ vs SAP-EV, &&&&$p < 0.0001$ vs SAP-EV+EV^{NCV}. Tukey's multiple comparisons test was used to analyze the differences between two groups). (B) ELISA data for IL-6 and TNFα levels in PMVEC culture supernatants after the indicated interventions (n = 6/group; ***$p < 0.001$, ****$p < 0.0001$ vs SC-EV, #$p < 0.05$ vs SAP-EV). (C) Representative transmission electron microscopy images of PMVEC junctions after incubation with SC-EV or SAP-EV with or without EV^{ITGB2}, EV^{ITGAM}, or EV^{NCV} (8 kV scale bar = 2 μm, 25 kV scale bar = 500 nm). (D) Western blot analysis and graphs of ICAM-1, VE-cadherin, and ZO-1 in PMVECs after the indicated interventions (n = 6/group; **$p < 0.01$, ***$p < 0.001$, ****$p < 0.0001$ vs SC-EV, ##$p < 0.01$, ###$p < 0.001$, ####$p < 0.0001$ vs SAP-EV).

SAP-specific increase in both these pancreatic-specific markers, including a SAP-specific increase in pancreas-derived serum EVs (Figure S3). Next, transgenic mice were injected with equal doses of EV^{ITGAM}, EV^{ITGB2}, or EV^{NCV} isolates after SAP induction and analyzed to evaluate the effect of exogenous EV ITGAM or ITGB2 expression on pulmonary SAP-EV accumulation and inflammation. These mice revealed a marked pulmonary accumulation of pancreatic EVs, which was

significantly reduced upon injection of EV^{ITGAM} or EV^{ITGB2}, but not EV^{NCV} samples as determined by red fluorescence signal in lung tissue (Figure 6A) or tissue sections of these mice (Figure S4). SAP mice injected with PBS or EV^{NCV} revealed similar lung histopathology scores increases, but the scores of EV^{ITGAM}-injected and EV^{ITGB2}-injected SAP mice did not significantly differ from those of SC mice (Figure 6B). Similarly, SAP mice revealed substantial injury to the pancreas,

kidney, liver, heart, spleen, and small intestines compared to SC mice. SAP mice injected with EV^{NCV} did not differ from those injected with PBS. However, SAP mice injected with EV^{ITGB2} and EV^{ITGAM} had significantly reduced renal injury, and SAP mice injected with EV^{ITGAM} had reduced injury to their small intestines (Figure S5). EV^{ITGAM}-injected and EV^{ITGB2}-injected SAP mice also revealed reduced disruption of PMVEC connections (Figure 6C) and attenuated pulmonary IL-6 and TNFα expression (Figure 6D) versus PBS-injected and EV^{NCV}-injected SAP mice. We next analyzed the relative pulmonary accumulation of PKH67-labeled EV^{ITGAM}, EV^{ITGB2}, and EV^{NCV} samples to determine if EV inhibitory effects reflected the pulmonary accumulation of the injected EVs. This analysis found that PKH67 green-fluorescent signal was increased in the lungs of EV^{ITGAM}-injected and EV^{ITGB2}-injected SAP mice but not EV^{NCV}-injected SAP mice whose PKH67 signal did not differ from that of SAP mice (Figure S6).

EV^{ITGB2} and EV^{ITGAM} Attenuate SAP-EV Effects on Cultured PMVECs. To directly evaluate EV^{ITGB2} and EV^{ITGAM} effects to attenuate SAP-EV-mediated phenotypes, PMVEC cultures were incubated with SC-EV, SAP-EV, or SAP-EV and EV^{ITGB2}, EV^{ITGAM}, or EV^{NCV} samples and evaluated for SAP-EV uptake, and SAP-EV-mediated dysregulation of cell contacts and their expression tight junctions and pro-inflammatory proteins. PMVECs demonstrated efficient uptake of both the mouse and cell culture EV fractions but greater uptake of the SAP-EV versus SC-EV fraction and greater uptake of EV^{ITGB2} and EV^{ITGAM} than EV^{NCV} fractions. SAP-EV uptake was also inhibited by treatment with EV^{ITGB2} and EV^{ITGAM} but not EV^{NCV} fractions (Figure 7A). Similarly, SAP-EV treatment stimulated PMVECs to secrete high levels of IL-6 and TNFα, and treatment with EV^{ITGB2} and EV^{ITGAM} but not EV^{NCV} attenuated this pro-inflammatory effect (Figure 7B). PMVECs incubated with SAP-EV revealed intercellular junction disruptions not detected after SC-EV incubation, and these SAP-EV-induced disruptions were attenuated when these cells were coincubated with SAP-EV and EV^{ITGB2} or EV^{ITGAM} but not EV^{NCV} fractions (Figure 7C). SAP-EV versus SC-EV incubation also decreased expression of the tight junction proteins VE-cadherin and ZO-1 and increased ICAM-1 expression, and PMVEC coincubation with EV^{ITGB2} and EV^{ITGAM} but not EV^{NCV} fractions attenuated this SAP-EV effect (Figure 7D). There thus appears to be inverse correspondence between SAP-EV accumulation and EV^{ITGB2} and EV^{ITGAM} accumulation both *in vitro* and *in vivo*, which is not observed in EV^{NCV}-treated mice or cell cultures. Given that a similar effect is also observed when SC mice are treated with SAP-EVs preincubated with the integrin blocking peptide HYD-1, we hypothesize that these effects are at least partly due to a competition for PMVEC surface binding sites by these EVs. Thus, it may be possible to attenuate or block SAP-EV-induced PMVEC injury and inflammation by exogenous administration of EV^{ITGB2} and EV^{ITGAM} therapy.

To summarize, we observed that serum EV levels were increased in a mouse SAP model with ALI versus a MAP model without ALI, which could arise from SAP-mediated inflammatory injury or induce ALI, as EVs can transmit information between adjacent or distant cells to alter their phenotypes.[16,36] SC and MAP mice injected with SAP-EVs demonstrated greater pulmonary EV accumulation and inflammation than those infected with MAP-EVs or SC-EVs. Comparison of the SAP-EV and MAP-EV proteomes found a

differential enrichment of ECM proteins, including several integrins that participate in cell adhesion;[37,38] the response to peptide hormones; and the acute-phase response that could mediate pulmonary inflammation. SAP-EV factors may thus promote pulmonary EV accumulation and inflammation. Serum EVs are primarily derived from red blood cells and platelets under normal physiologic conditions. However, Jiménez-Alesanco *et al.* have reported that EVs of a rat SAP model exhibit increased serum expression of two pancreas-derived proteins (amylase and chimotrypsinogen).[39] Similarly, our results indicate that serum EVs of SAP mice exhibit increased expression of the pancreas-specific protein pdx1 and more EVs positive for pdx-driven tdTomato fluorescence than SC and MAP mouse EVs. These results imply that the serum abundance of pancreas-derived EVs increases in SAP mice but not MAP mice, even though both these groups exhibit significant, if unequal, serum EV increases.

Viruses and bacteria can directly mediate lung inflammation leading to ALI by injuring alveolar epithelial cells,[40] but the mechanism(s) responsible for regulating lung injury responses in the absence of pathogen action are less clear. We have previously reported that SAP-EVs can promote the pro-inflammatory polarization of alveolar macrophages and the secretion of inflammatory factors (TNFα, NO, MIP-2) that can participate in the development of ALI.[41] However, circulating SAP-EVs must first contact PMVECs and enter pulmonary tissue to affect alveolar macrophages. We now report that SAP-EV can regulate lung injury by direct effects to promote inflammation in lung endothelial cells and damage their barrier function—the earliest pathological event in SAP-induced ALI development[17]—by increasing their secretion of the pro-inflammatory factors IL-6 and TNFα, down-regulating their expression of the tight junction proteins VE-cadherin and ZO-1, and up-regulating their expression of intercellular adhesion molecule (ICAM-1).

EVs demonstrate enriched expression of several membrane proteins, including tetraspanins, integrins, and major histocompatibility complex (MHC) proteins that can have functional importance.[16,42] Notably, integrins expressed on tumor-derived EVs are reported to contribute to tumor organotropism.[42,43] For example, integrins $\alpha 6\beta 1$ and $\alpha 6\beta 4$ are enriched on EVs that can promote lung metastasis, while EV $\alpha v\beta 5$ expression is closely associated with liver metastasis.[18] We observed that ITGAM and ITGB2 are enriched on SAP-EVs but not NC or MAP-EVs in our mouse studies. Similar results were obtained when we analyzed ITGAM and ITGB2 protein expression on serum EVs obtained from a small cohort containing six healthy negative control subjects (NC), six patients with MAP, and six patients with SAP. ITGAM and ITGB2 were significantly enriched on serum EVs of SAP when compared to their expression on NC subjects, but potential increases detected in MAP patients did not significantly differ from expression in NC subjects (Figure S7). And, HYD-1-mediated integrin blockade prevented lung accumulation of SAP-EVs in healthy mice and the development of SAP-ALI-related lung pathology. We also found that EV^{ITGB2} and EV^{ITGAM} exhibited greater lung accumulation than EV^{NCV} and inhibited SAP-EV lung accumulation, potentially *via* direct competition for binding sites on PMVECs or by reducing lung expression of these receptors. Mice injected with EV^{ITGB2} and EV^{ITGAM} or PMVEC cultures incubated with these EVs are partially protected from SAP-EV effects. Thus, SAP-EVs appear to target PMVEC through integrin-mediated mecha-

nisms to promote their accumulation in lung tissue where they induce endothelial injury and inflammation responses that can damage the PMVEC barrier. These findings are comparable to those of a study that found that EVs that highly express the SARS-CoV-2 receptor ACE2 can competitively inhibit SARS-CoV-2 interaction with host cells to inhibit SARS-CoV-2 effects on the lungs.[44,45]

ITGAM and ITGB2 heterodimerize to form integrin $\alpha m\beta 2$ (Mac-1), which is involved in cell migration and adhesion. ITGB2 can mediate interactions between neutrophils and endothelial cells that can disrupt endothelial cell function through the transfer of myeloperoxidase (MPO) in atherosclerosis and vasculitis diseases,[46] ITGAM can promote the development of abdominal aorta aneurysms by mediating endothelial cell adhesion and the cross-endothelial migration of circulating monocytes/macrophages.[47] Our results indicate that SAP-EVs, which highly expressed ITGB2 and ITGAM, disrupt lung endothelial cell tight junctions to permit pro-inflammatory factors and activated immune cells to enter the alveolar cavity and stimulate ICAM-1 expression that can recruit more pro-inflammatory cells to amplify the inflammatory response and further promote SAP-ALI development.[48] Notably, EV^{ITGB2} or EV^{ITGAM} treatment was found to competitively block SAP-EV adhesion to PMVECs and maintained their barrier function to inhibit SAP-ALI progression. These findings indicate that ITGB2 and ITGAM mediate the PMVEC targeting activity of SAP-EVs but not their activity to induce PMVEC barrier damage and inflammatory response, implying that other factors carried by SAP-EVs regulate these processes. Further studies are required to identify which factors may mediate these injury and inflammation phenotypes, although our preliminary data suggest that SAP-EV-mediated transfer of S100A9 mRNA may play a role in these processes.

Comparison of SAP-EV and SC-EV protein cargoes by mass spectrometry found that the inflammatory protein S100A9 was significantly up-regulated in SAP-EVs, ranking in the top 20 differentially expressed proteins. Notably, S100A9 is highly expressed in the pancreatic tissue of rats with acute pancreatitis.[49] Serum EVs of patients with SAP also contain high S100A9 levels that can promote a multiorgan inflammatory response by activating NADPH oxidase to produce free radicals and can be used to predict disease severity.[49,50] Similarly, in a mouse sepsis model, S100A9 participates in and mediates lung injury by promoting neutrophil activation and lung accumulation and blocking its function can improve sepsis-induced ALI.[51] We thus hypothesized that SAP-EV S100A9 protein plays an important role in SAP-ALI.

To test this hypothesis, we incubated SAP-EVs with and without S100A9-specific siRNA ($S100A9^{-/-}$-SAP-EVs and control-SAP-EVs, respectively) and then injected these EVs into healthy mice that were subsequently evaluated for lung pathology and expression of inflammatory factors. Only 10% of the $S100A9^{-/-}$-SAP-EVs revealed detectable evidence of siRNA uptake (Figure S8), but lung pathology scores and IL-6 and TNFα expression levels were significantly reduced in mice injected with $S100A9^{-/-}$-SAP-EVs versus control-SAP-EVs, suggesting that S100A9 mRNA transferred by SAP-EVs contributed to the process of SAP-ALI. However, further studies are needed to confirm this data and evaluate the potential roles that other SAP-EV factors may play in SAP-ALI.

Further, the HEK293T cell line used to generate EV^{NCV}, EV^{ITGB2}, and EV^{ITGAM} isolates used in cell culture and mouse studies have low immunogenicity and toxicity and may carry factors that mitigate the pro-inflammatory responses induced by SAP-EVs.[52] Further studies are thus also necessary to determine if specific factors in these EVs mediate their effects to attenuate SAP-EV-mediated cell injury and inflammation effects, and the mechanisms responsible for these processes, or whether these effects are mediated by receptor competition alone. However, taken together, our results indicate that EVs or other nanoparticles engineered to express ITGB2 and ITGAM on their surface could serve as promising therapeutics to prevent or attenuate SAP-ALI responses.

CONCLUSIONS

In summary, our results demonstrate that SAP-EVs: employ an integrin-mediated interaction to adhere to PMVEC; disrupt their barrier function, with a corresponding attenuation of their expression of the tight junction proteins VE-cadherin and ZO-1; and promote their secretion of pro-inflammatory IL-6 and TNFα. Blocking this interaction by pretreating SAP-EVs with HYD-1 or by injecting mice with EV^{ITGB2} and EV^{ITGAM} prevented lung tissue SAP-EV accumulation and injury, indicating that this interaction plays a key role in SAP-ALI and strongly suggests that interventions that employ new therapeutic agents, such as engineered EVs, could have beneficial effects to attenuate the development, progression, and high early mortality of SAP-ALI.

EXPERIMENTAL SECTION

Mouse MAP and SAP Model Establishment. The protocol of animal experiments was approved by the Animal Care and Use Committee of West China Hospital (Permit No. 2020233A). A mouse model of SAP was established by retrograde injection of 2% taurocholic acid sodium salt hydrate (T4009, Sigma) into the pancreatic duct. C57BL/6 mice about 25 g in size were anesthetized by isoflurane (R510-22, RWD Life Science Co., Ltd., Shenzhen, China), and then, the mice were fixed in the supine position. A midline laparotomy was performed to find the pancreas and duodenal papilla. The puncture wound was caused by using the arrow of 24 G venous indwelling needle (Weihai Jierui Medical Products Co., Ltd., Shandong, China) at the mesenteric margin of the duodenum. The puncture wound followed the duodenum into the pancreatic duct, and then, the pancreatic duct near the hepatic hilus was clamped with a microvascular clamp. The 2% taurocholic acid sodium salt hydrate was pumped through the intravenous indwelling needle with a micro pump (Lande Medical Equipment Co., Ltd., Shanghai, China) at the rate of 0.06 mL/h for 4 min. After the infusion was completed, the catheter and vascular clamp were removed. The duodenal puncture wound was sutured with a 7-0 suture line. Finally, the abdomen was closed and sutured. About 0.8 mL of normal saline was injected subcutaneously to prevent dehydration. After the mice were rewarmed, the mice were put into a cage.

MAP (mild acute pancreatitis) mice were established by intraperitoneal injection of caerulein (60321ES03, Yeasen Biotechnology Co., Ltd., Shanghai, China). C57BL/6 male mice (22−24 g) were fed adaptively for 1 week, fasted for 12h before operation, and drank freely. Then, the MAP mice model was established by intraperitoneal injection of 50 $\mu g/kg$ caerulein for seven consecutive times, each time with an interval of 1 h. After 24 h of modeling, all mice were killed by overdose anesthesia to collect serum and lung tissue samples.

Histopathological Examination and Pathological Score. After fixation with 4% paraformaldehyde, lung tissues were embedded in paraffin and made into sections (5 μm thick). Hematoxylin and eosin (H&E) staining of sections were carried out. The tissue sections were first dewaxed with xylene and then placed in different concentration gradients of alcohol (high to low) to wash away the xylene. Hematoxylin staining was performed for 5 min, followed by

color separation with hydrochloric acid ethanol and then staining with 5% eosin solution for 2−3 min. Then, the tissue was dehydrated with different concentration gradient ethanol (from low concentration to high concentration) and made transparent with xylene. Finally, neutral gum was dropwise added, and the mixture was covered with a cover glass for sealing. An image of the stained sections was acquired using a Pannoramic Digital Slide Scanners (3D HISTECH).

The degree of acute lung injury was evaluated using four parameters: interstitial and alveolar edema, hemorrhage, inflammatory cell infiltration, and fibrosis (thickening of alveolar wall). Each was graded on a 5-point scale: (0) minimum damage, (1) slight damage, (2) moderate damage, (3) serious damage, and (4) maximum damage. The four sores were summed to determine the pathological score of the lung tissue.

Isolation of EVs. ExoQuickTM Exosome Precipitation Solution (EXOQ5A, System Biosciences, Palo Alto, CA) was used to isolate EVs from serum using the manufacturer's protocol.

For HEK293T EV isolation, HEK293T cells were transfected with plasmid, washed twice with PBS, and switched to serum-free medium. HEK293T cells were cultured in a serum-free medium at 37 °C in 5% CO_2 for 48 h, after which culture supernatant was collected for EV isolation. Briefly, cell culture medium was centrifuged at 2000g for 20 min at 4 °C to remove large cell debris and the supernatant was collected and centrifuged at 12,000g for 45 min at 4 °C to remove small cellular debris. The supernatant was then centrifuged at 120,000g for 75 min at 4 °C; then, the supernatant was discarded, and the precipitate was resuspended with cold PBS, and filtered with a 0.22 μm filter. This filtrate was then centrifuged at 120,000g at 4 °C for 75 min, the supernatant was discarded, and the EV precipitate was collected.

Nanoparticle Tracking Analysis (NTA). NTA of EVs samples was carried out using a Zeta View PMN 120 (Particle Metrix, Meerbusch, Germany). Briefly, EVs were diluted (v/v, 1:1000 or 1:2000) with pure water, and their size distributions and particle concentration were analyzed using the parameters (min area 5, max area 1000, sensitivity 70, shutter 70, and min brightness 20) at 25 °C.

Transmission Electron Microscopy (TEM). The morphology of EVs, lung tissues, and mouse pulmonary microvascular endothelial cells (PMVECs) was evaluated using a TEM (JEM-1400FLASH, JEOL, Tokyo, Japan) at voltages of 8 and 25 kV. The freshly extracted EVs were directly dropped onto the copper mesh, and after 1 min, uranyl acetate was dropped onto the copper mesh for precipitation for 1 min. The EVs were dried at room temperature and detected and imaged under electron microscopy at 8 and 25 kV.

For lung tissues and PMVECS, the lung tissues were isolated immediately and fixed in the 3% glutaraldehyde, and mouse PMVECs were digested with trypsin, and then, the cell precipitate was collected. The cells were fixed with 0.5% glutaraldehyde solution for 10 min and then fixed with 3% glutaraldehyde solution. These samples were postfixed in 1% osmium tetroxide, dehydrated in series acetone, infiltrated in Epox 812 for a longer, and embedded. The semithin sections were stained with methylene blue, and ultrathin sections were cut with diamond knife and stained with uranyl acetate and lead citrate. Sections were examined with a JEM-1400-FLASH transmission electron microscope.

Isolation of Primary Mouse PMVECs. Mouse PMVECs were isolated using a magnetic bead sorting method. Single cells were prepared from mouse lung tissue using a mouse lung dissociation kit (cat. no.130-095-927, Miltenyi Biotec). CD45-CD90.2-CD326 cells were screened by depletion with CD45 MicroBeads (cat. no. 130-052-301, Miltenyi Biotec), CD90.2 MicroBeads (cat. no. 130-121-278, Miltenyi Biotec), and CD326 MicroBeads (cat. no.130-105-958, Miltenyi Biotec). Adherent mouse PMVECs were cultured in DMEM-F12 medium containing 1% endothelial cell growth supplement (SC1052, ScienCell), 1% penicillin−streptomycin solution (BC-CE-007, Biochannel, Nanjing, China), and 10% fetal bovine serum (10099141, Gibco) in a T25 cell culture flask in a humidified incubator (37 °C, 5% CO_2).

Tracking of EVs in Vivo and in Vitro. Extracted mouse plasma EVs were resuspended with sterile 1 × PBS. In peptide blocking

experiments, EVs were incubated with 75 μg/mL HYD-1 (peptide sequence: KIKMVISWKG) peptides for 30 min at 37 °C before EV fluorescent staining and injection. For the in vivo analysis of the EV distribution, the EVs were incubated in the dark with DIR (UR21017, Umibio Co., Ltd., Shanghai, China) at 37 °C for 30 min. The samples were then processed using the EV isolation method to remove excess dye, and 100 μg of stained EVs was injected into the tail vein of ∼20 g mice, with the same volume of DIR diluent and PBS injected into the tail veins of control mice. After 24 h, the mice were euthanized by intraperitoneal injection of 5% pentobarbital sodium (4 mg/kg). Lung tissue was harvested and imaged using an IVIS spectrum in vivo imaging system (IVIS Lumina II, PerkinElmer). The fluorescence intensity in the lung tissue was analyzed using the IVIS software (Ex/Em: 748/780 nm, Living Image Software for IVIS).

For cellular EV uptake analysis, SC-EVs, SAP-EVs, and HYD-EVs were labeled with PKH26 (UR52302, Umibio Co., Ltd., Shanghai, China) and engineered EVs (EV^{NCV}, EV^{ITGB2}, and EV^{ITGAM}) were labeled with PKH67 (UR52303, Umibio Co., Ltd., Shanghai, China). First, the PKH26/PKH67 linker was diluted with Diluent C in a ratio of 1:9, and then, the PKH26/PKH67 staining working solution (v/v, 1:10) was added into the corresponding EV solution to be fully mixed and allowed to stand for incubation for 10 min. These EVs were then processed using the EV isolation method to remove excess dye using aseptic technique, and stained EVs were resuspended in 200 μL od 1 × PBS. For SAP-EV integrin block experiment, adherent PMVECs were incubated with 20 μg/mL SC-EV, SAP-EV, and HYD-EV for 24 h. After the incubation, the cells were washed three times with PBS and fixed with 4% paraformaldehyde at room temperature for 30 min. After staining with DAPI (C0065, Solarbio Life Science, Beijing, China) for 10 min and Phallodin (40736ES75, Yeasen Biotechnology Co., Ltd., Shanghai, China) for 10 min, the sections were sealed and observed under a confocal microscope (N-SIM S, Nikon).

In another cell experiment, adherent PMVECs were incubated with 20 μg/mL SC-EV or SAP-EV with or without 20 μg/mL EV^{NCV}, EV^{ITGB2}, and EV^{ITGAM} for 24 h. After the incubation, the cells were washed three times with PBS and fixed with 4% paraformaldehyde at room temperature for 30 min. After staining with DAPI (C0065, Solarbio Life Science, Beijing, China) for 10 min, the sections were sealed and observed under a confocal microscope (N-SIM S, Nikon).

Immunofluorescence (IF) Staining. Lung tissue of mice injected with DIR-labeled EVs was paraffin embedded and sectioned (5 μm), dewaxed, and hydrated in different concentrations of ethanol. Sections were treated with 3% hydrogen peroxide at room temperature for 30 min to quench endogenous peroxidase activity and then washed with PBS. Sections were then placed in 10 mmol/L citrate buffer (pH = 6.0, 94 °C) for 10 min, and the sections were incubated with the blocking solution at room temperature for 1 h to block the nonspecific sites. Sections were then incubated with primary antibody CD68 (ab201340, Abcam, Milton, UK) or vWF (ab287962, Abcam, Milton, UK) or SPC (DF6647, Affinity Biosciences) or S100A4 (ab197896, Abcam, Milton, UK) at 4 °C overnight (about 12 h). After three washings, the sections were incubated with the appropriate fluorescent secondary antibody (FITC) at room temperature for 50 min and then washed in PBS for 3 times, each time for 5 min. After slicing, DAPI dye solution was dripped into the circle and incubated for 3−5 min at room temperature in the dark. Finally, the sections were placed under fluorescence microscope for observation (wavelengths: 450−480, 500−560, and 605−625 nm) and the images were taken.

Analysis of Cytokine Levels in Lung Tissues and PMVECs Cell Supernatant. Dilution buffer was added into lung tissue at a 1:9 ratio, tissue was ground, and supernatants were collected for analysis. Cell culture supernatants for PMVECs were collected after 24 h of EVs intervention. Test samples were prepared using mouse interleukin 6 (IL-6) and tumor necrosis factor a (TNFα) ELISA kits (DLDEVELOP) according to the manufacturer's protocol and read at 450 nm immediately.

Proteomic Analysis of Plasma EVs. Mouse plasma EVs were isolated from the sham, MAP, and SAP mouse groups were lysed on ice for 30 min, protein concentrations were determined by

Bicinchoninic Acid (BCA) (P0010S, Beyotime Biotechnology, Shanghai, China) method, and the protein quality was determined by sodium dodecyl sulfate polyacrylamide gel electrophoresis (SDS-PAGE) (Sinopharm Chemical Reagent Co., Ltd., Shanghai, China). The protein samples whose quality meet the standard were subjected to reductive alkylation, trypsin digestion, and then labeled with a tandem mass tag (TMT) reagent (A44522, ThermoFisher, San Jose, CA) to differentially label peptides from each sample. These labeled peptides were then mixed in equal amounts, preseparated by C18 reversed-phase column (Acquity UPLC BEH C18 column 1.7 m, 2.1 mm × 150 mm, Waters), and analyzed by liquid chromatography coupled with tandem mass spectrometry (LC−MS/MS) (Orbitrap Exploris 480, ThermoFisher, San Jose, CA). The Sequest or Mascot module in Proteome Discoverer was used for database searches, and data statistics and bioinformatics analysis were determined for the search results.

Western Blotting. Samples (lung tissue or lung vascular endothelial cells) were dissolved in lysis buffer for lysis, centrifuged at 12,000g for 5 min to collect their supernatants, and analyzed for their protein concentration using a BCA kit. High-resolution separation of protein samples (20 or 40 μg protein/well) was obtained on a 12% SDS-PAGE gel. These proteins were then transferred to nitrocellulose or PVDF membranes (Milipore). These membranes were blocked for 10 min at room temperature using a commercial blocking solution (PS108, Epizyme Biotech, Shanghai, China), washed three times with TBST, and incubated with VE-cadherin (1:1000, ab205336, Abcam), ZO-1 (1:1000, ab216880, Abcam), ICAM-1 (1:1000, ab222736, Abcam), β-catenin (1:20000, Affinity), ITGAM (1:1000, #17800, CST), ITGB2 (1:1000, #72607, CST), TSG101 (1:1000, ab125011, Abcam), CD9 (1:1000, A1703, Abclonal), Calnexin (1:1000, ab227310, Abcam), and Syntenin (1:1000, ab19903, Abcam), overnight at 4 °C (approximately 12 h). These membranes were then washed three times with TBST and incubated with a fluorescently labeled secondary antibody (antirabbit or antimouse IgG, Cell Signaling Technology) for 60 min at room temperature. After three washes, the prints were visualized using an imaging system (Bio-Rad).

Genetic Modification of HEK293T Cells. The plasmids pCMV3-HA-mITGB2 (Catalog: MG50359-NY), pCMV3-mIT-GAM-t2-Flag (Catalog: MG57042-CF), and pCMV3-C-Flag-NCV (Catalog: CV012) were purchased from Sino Biological Inc. (Beijing, China). HEK293T cells (CRL-11268, ATCC) were collected by 0.25% Trypsin (with EDTA) digestion, seeded on 10 cm cell culture dish in DMEM medium with 10% fetal bovine serum (HyClone) at a density of 2×10^7 cells/dish, and incubated in 37 °C incubator containing 5% CO_2 for 8 h. Turbofect-DNA transfection reagents [10 μg of plasmid DNA, 20 μL of Turbofect (R0531, Thermo Fisher), and 1000 μL of Opti-Medium (51985034, Gibco)] were prepared and added dropwise to the cell culture medium of the monolayers mentioned above and incubated overnight in a 37 °C incubator containing 5% CO_2. The supernatant was then removed and replaced with DMEM medium preheated at 37 °C containing 10% serum without EV. The cells were cultured for 48 h, and the cell supernatant was collected for extraction of EV and cell pellet for gene identification.

Rosa26-LSL-tdtomato x Pdx1-cre Mouse. Mice with pancreatic-specific fluorescent (ROSA26-LSL-tdtomato x Pdx1-cre) were generated by crossing PDX1-CRE mice and Rosa26-LSL-TDTomato (LoxP silenced) mice purchased from Shanghai Model Organisms Company (Shanghai, China). Genomic DNA was extracted from 12−19-day old mouse tails using the fast tissue-to-PCR kit (K1091, Fermentas) and PCR-analyzed using the following primers from Thermo Fisher Scientific: Pdx1-Cre-F, CCTGGACTACATCTT-GAGTTGC; Pdx1-Cre-R, AGGCAAATTTTGGTGTACGG; Rosa26-LSL-tdtomato-F1, AAGGGAGCTGCAGTGGAGTA; Rosa26-LSL-tdtomato-R1, CCGAAAATCTGTGGGAAGTC; Rosa26-LSL-tdtomato-F2, GGCATTAAAGCAGCGTATCC; Rosa26-LSL-tdtomato-R1, CTGTTCCTGTACGGCATGG. PCR was performed in 20 μL of reaction volume containing 10 μL of Taq Plus master mix (2X) (P212, Vazyme), 0.5 μM forward and reverse primers, 4 μL of genomic DNA, and 6 or 7 μL of ddH$_2$O. The PCR reaction was carried out in a thermal cycler as follows: initial denaturation for 3 min at 94 °C, followed by 35 cycles of denaturation for 30 s at 94 °C, annealing for 30 s at 58 °C, extension for 30 s at 72 °C, and a final extension of 5 min at 72 °C. The samples as were than cooled to 12 °C. Genotypes were visualized by 1.5% agarose gel. The marker was 100bp DNA Ladder Marker from Takara (3422A).

Statistical Analysis. All data are presented as the means ± standard deviations and statistically analyzed using GraphPad Prism 9 (GraphPad Software). Student's t test or one-way analysis of variance (ANOVA) followed by Tukey's multiple comparisons tests to compare the differences between two groups or intergroup differences. $P < 0.05$ was considered to be significant.

ASSOCIATED CONTENT

S1 Supporting Information

The Supporting Information is available free of charge at https://pubs.acs.org/doi/10.1021/acsnano.2c12722.

> Figures of distribution and effect of SAP-EV on lung tissue *in vivo*, Western blot analysis and graphs of ITGAM and ITGB2 expression on serum EVs isolated from clinically healthy negative control subjects (NC) and patients with mild acute pancreatitis (MAP) and severe acute pancreatitis (SAP), and role of S100A9 gene on SAP-EV in acute lung injury (PDF)

AUTHOR INFORMATION

Corresponding Author

Meihua Wan − *Department of Integrated Traditional Chinese and Western Medicine, West China Hospital of Sichuan University, Chengdu 610041, China; West China Hospital (Airport) of Sichuan University, Chengdu 610299, China;* orcid.org/0000-0002-1237-9455; Email: wanmh@scu.edu.cn

Authors

Qian Hu − *Department of Integrated Traditional Chinese and Western Medicine, West China Hospital of Sichuan University, Chengdu 610041, China*

Shu Zhang − *Department of Emergency Medicine, Emergency Medical Laboratory, West China Hospital of Sichuan University, Chengdu 610041, China*

Yue Yang − *Department of Integrated Traditional Chinese and Western Medicine, West China Hospital of Sichuan University, Chengdu 610041, China*

Juan Li − *Department of Integrated Traditional Chinese and Western Medicine, West China Hospital of Sichuan University, Chengdu 610041, China*

Hongxin Kang − *Department of Integrated Traditional Chinese and Western Medicine, West China Hospital of Sichuan University, Chengdu 610041, China*

Wenfu Tang − *Department of Integrated Traditional Chinese and Western Medicine, West China Hospital of Sichuan University, Chengdu 610041, China*

Christopher J. Lyon − *Center of Cellular and Molecular Diagnosis, Tulane University School of Medicine, New Orleans, Louisiana 70112, United States; Department of Biochemistry & Molecular Biology, Tulane University School of Medicine, New Orleans, Louisiana 70112, United States*

Complete contact information is available at:
https://pubs.acs.org/10.1021/acsnano.2c12722

Author Contributions

Q.H. interpreted the experimental data and prepared the manuscript draft. W.T. and M.W. conceived the research and designed the experiments. Y.Y. and Q.H. performed the experiments. S.Z. was responsible for collecting clinical samples and analyzing the data. J.L. and H.K. analyzed the date. C.J.L. and M.W. finalized the manuscript. All authors have given approval to the final version of the manuscript.

Funding

Notes

The authors declare no competing financial interest.

ACKNOWLEDGMENTS

ABBREVIATIONS USED

ACE2, angiotensin-converting enzyme 2; ALI, acute lung injury; AP, acute pancreatitis; AMPK, adenosine 5′-monophpsphate-activated protein kinase; CCL2, C−C motif chemokine ligand 2; ECM, extracellular matrix; H&E, hematoxylin and eosin; HEK293T cells, human embryonic kidney 293T cells; ICAM-1, intercellular cell adhesion molecule-1; ILK, integrin-linked kinase; ITGA2B, integrin αIIb; ITGAM, integrin α M; ITGB2, integrin β2; LCSs, lung spherical cells; LPS, lipopolysaccharide; Mac-1, macrophage-1 antigen; MAP, mild acute pancreatitis; MHC, major histocompatibility complex; MPO, myeloperoxidase; NTA, nanoparticle tracking analysis; PCA, principal component analysis; PMVECs, pulmonary microvascular endothelial cells; ROS, reactive oxygen species; S100A4, S100 calcium binding protein A4; SAP, severe acute pancreatitis; SPC, surfactant protein C; SDS-PAGE, sodium dodecyl sulfate polyacrylamide gel electrophoresis; TEM, transmission electron microscopy; TGFβ, transforming growth factor; TMT, tandem mass tag; TNFα, tumor necrosis factor-α; VE-cadherin, vascular endothelial cell cadherin; VEGF, vascular endothelial growth factor; ZO-1, zonulaoccludens-1

REFERENCES

(1) Habtezion, A.; Gukovskaya, A. S.; Pandol, S. J. Acute Pancreatitis: A Multifaceted Set of Organelle and Cellular Interactions. *Gastroenterology* 2019, 156 (7), 1941−1950.

(2) Banks, P. A.; Bollen, T. L.; Dervenis, C.; Gooszen, H. G.; Johnson, C. D.; Sarr, M. G.; Tsiotos, G. G.; Vege, S. S. Classification of acute pancreatitis–2012: revision of the Atlanta classification and definitions by international consensus. *Gut* 2013, 62 (1), 102−11.

(3) Mederos, M. A.; Reber, H. A.; Girgis, M. D. Acute Pancreatitis: A Review. *Jama* 2021, 325 (4), 382−390.

(4) Lei, H.; Minghao, W.; Xiaonan, Y.; Ping, X.; Ziqi, L.; Qing, X. Acute lung injury in patients with severe acute pancreatitis. *Turkish journal of gastroenterology: the official journal of Turkish Society of Gastroenterology* 2013, 24 (6), 502−7.

(5) Owusu, L.; Xu, C.; Chen, H.; Liu, G.; Zhang, G.; Zhang, J.; Tang, Z.; Sun, Z.; Yi, X. Gamma-enolase predicts lung damage in severe acute pancreatitis-induced acute lung injury. *Journal of molecular histology* 2018, 49 (4), 347−356.

(6) Landahl, P.; Ansari, D.; Andersson, R. Severe Acute Pancreatitis: Gut Barrier Failure, Systemic Inflammatory Response, Acute Lung Injury, and the Role of the Mesenteric Lymph. *Surgical infections* 2015, 16 (6), 651−6.

(7) Liu, D.; Wen, L.; Wang, Z.; Hai, Y.; Yang, D.; Zhang, Y.; Bai, M.; Song, B.; Wang, Y. The Mechanism of Lung and Intestinal Injury in Acute Pancreatitis: A Review. *Frontiers in medicine* 2022, 9, 904078.

(8) Zhu, X.; Duan, F.; Zhang, Y.; Wang, X.; Wang, Y.; Chen, J.; Zhang, L.; Wu, M.; Pan, Z.; Chen, B. Acadesine alleviates acute pancreatitis-related lung injury by mediating the barrier protective function of pulmonary microvascular endothelial cells. *International immunopharmacology* 2022, 111, 109165.

(9) Vege, S. S.; DiMagno, M. J.; Forsmark, C. E.; Martel, M.; Barkun, A. N. Initial Medical Treatment of Acute Pancreatitis: American Gastroenterological Association Institute Technical Review. *Gastroenterology* 2018, 154 (4), 1103−1139.

(10) Tsuchiya, T.; Doi, R.; Obata, T.; Hatachi, G.; Nagayasu, T. Lung Microvascular Niche, Repair, and Engineering. *Front. Bioeng. Biotechnol.* 2020, 8, 105.

(11) Hu, Q.; Zhang, S.; Yang, Y.; Yao, J. Q.; Tang, W. F.; Lyon, C. J.; Hu, T. Y.; Wan, M. H. Extracellular vesicles in the pathogenesis and treatment of acute lung injury. *Military Med.Res.* 2022, 9 (1), 61.

(12) Stevens, T. Functional and molecular heterogeneity of pulmonary endothelial cells. *Proceedings of the American Thoracic Society* 2011, 8 (6), 453−7.

(13) Li, L.; Wei, J.; Mallampalli, R. K.; Zhao, Y.; Zhao, J. TRIM21 Mitigates Human Lung Microvascular Endothelial Cells' Inflammatory Responses to LPS. *American journal of respiratory cell and molecular biology* 2019, 61 (6), 776−785.

(14) Wang, Y.; Liu, S.; Li, L.; Li, L.; Zhou, X.; Wan, M.; Lou, P.; Zhao, M.; Lv, K.; Yuan, Y.; Chen, Y.; Lu, Y.; Cheng, J.; Liu, J. Peritoneal M2 macrophage-derived extracellular vesicles as natural multitarget nanotherapeutics to attenuate cytokine storms after severe infections. *Journal of controlled release: official journal of the Controlled Release Society* 2022, 349, 118−132.

(15) Jiang, J.; Huang, K.; Xu, S.; Garcia, J. G. N.; Wang, C.; Cai, H. Targeting NOX4 alleviates sepsis-induced acute lung injury via attenuation of redox-sensitive activation of CaMKII/ERK1/2/MLCK and endothelial cell barrier dysfunction. *Redox biology* 2020, 36, 101638.

(16) Hu, Q.; Su, H.; Li, J.; Lyon, C.; Tang, W.; Wan, M.; Hu, T. Y. Clinical applications of exosome membrane proteins. *Precis Clin Med.* 2020, 3 (1), 54−66.

(17) Wang, F.; Lu, F.; Huang, H.; Huang, M.; Luo, T. Ultrastructural changes in the pulmonary mechanical barriers in a rat model of severe acute pancreatitis-associated acute lung injury. *Ultrastructural pathology* 2016, 40 (1), 33−42.

(18) Hoshino, A.; Costa-Silva, B.; Shen, T. L.; Rodrigues, G.; Hashimoto, A.; Tesic Mark, M.; Molina, H.; Kohsaka, S.; Di Giannatale, A.; Ceder, S.; Singh, S.; Williams, C.; Soplop, N.; Uryu, K.; Pharmer, L.; King, T.; Bojmar, L.; Davies, A. E.; Ararso, Y.; Zhang, T.; Zhang, H.; Hernandez, J.; Weiss, J. M.; Dumont-Cole, V. D.; Kramer, K.; Wexler, L. H.; Narendran, A.; Schwartz, G. K.; Healey, J. H.; Sandstrom, P.; Labori, K. J.; Kure, E. H.; Grandgenett, P. M.; Hollingsworth, M. A.; de Sousa, M.; Kaur, S.; Jain, M.; Mallya, K.; Batra, S. K.; Jarnagin, W. R.; Brady, M. S.; Fodstad, O.; Muller, V.; Pantel, K.; Minn, A. J.; Bissell, M. J.; Garcia, B. A.; Kang, Y.; Rajasekhar, V. K.; Ghajar, C. M.; Matei, I.; Peinado, H.; Bromberg, J.; Lyden, D. Tumour exosome integrins determine organotropic metastasis. *Nature* 2015, 527 (7578), 329−335.

(19) Eliceiri, B. P.; Puente, X. S.; Hood, J. D.; Stupack, D. G.; Schlaepfer, D. D.; Huang, X. Z.; Sheppard, D.; Cheresh, D. A. Src-mediated coupling of focal adhesion kinase to integrin alpha(v)beta5 in vascular endothelial growth factor signaling. *J. Cell Biol.* 2002, 157 (1), 149−60.

(20) McCurley, A.; Alimperti, S.; Campos-Bilderback, S. B.; Sandoval, R. M.; Calvino, J. E.; Reynolds, T. L.; Quigley, C.; Mugford, J. W.; Polacheck, W. J.; Gomez, I. G.; Dovey, J.; Marsh, G.; Huang, A.; Qian, F.; Weinreb, P. H.; Dolinski, B. M.; Moore, S.; Duffield, J. S.; Chen, C. S.; Molitoris, B. A.; Violette, S. M.; Crackower, M. A. Inhibition of αvβ5 Integrin Attenuates Vascular

Permeability and Protects against Renal Ischemia-Reperfusion Injury. *Journal of the American Society of Nephrology: JASN* **2017**, *28* (6), 1741−1752.

(21) Chan, Y. C.; Leung, P. S. Acute pancreatitis: animal models and recent advances in basic research. *Pancreas* **2007**, *34* (1), 1−14.

(22) Grigoryeva, E. S.; Savelieva, O. E.; Popova, N. O.; Cherdyntseva, N. V.; Perelmuter, V. M. Do tumor exosome integrins alone determine organotropic metastasis? *Molecular biology reports* **2020**, *47* (10), 8145−8157.

(23) Chen, W.; Garcia, J. G.; Jacobson, J. R. Integrin beta4 attenuates SHP-2 and MAPK signaling and reduces human lung endothelial inflammatory responses. *Journal of cellular biochemistry* **2010**, *110* (3), 718−24.

(24) Jiang, L.; Wang, M.; Lin, S.; Jian, R.; Li, X.; Chan, J.; Dong, G.; Fang, H.; Robinson, A. E.; Snyder, M. P.; et al. A Quantitative Proteome Map of the Human Body. *Cell* **2020**, *183* (1), 269−283.

(25) Górska, A.; Mazur, A. J. Integrin-linked kinase (ILK): the known vs. the unknown and perspectives. *Cell. Mol. Life Sci.* **2022**, *79* (2), 100.

(26) Sroka, T. C.; Pennington, M. E.; Cress, A. E. Synthetic D-amino acid peptide inhibits tumor cell motility on laminin-5. *Carcinogenesis* **2006**, *27* (9), 1748−57.

(27) Sroka, T. C.; Marik, J.; Pennington, M. E.; Lam, K. S.; Cress, A. E. The minimum element of a synthetic peptide required to block prostate tumor cell migration. *Cancer biology & therapy* **2006**, *5* (11), 1556−62.

(28) Tornavaca, O.; Chia, M.; Dufton, N.; Almagro, L. O.; Conway, D. E.; Randi, A. M.; Schwartz, M. A.; Matter, K.; Balda, M. S. ZO-1 controls endothelial adherens junctions, cell-cell tension, angiogenesis, and barrier formation. *J. Cell Biol.* **2015**, *208* (6), 821−38.

(29) Zhang, X.; Wu, D.; Jiang, X. Icam-1 and acute pancreatitis complicated by acute lung injury. *JOP* **2009**, *10* (1), 8−14.

(30) Blight, B. J.; Gill, A. S.; Sumsion, J. S.; Pollard, C. E.; Ashby, S.; Oakley, G. M.; Alt, J. A.; Pulsipher, A. Cell Adhesion Molecules are Upregulated and May Drive Inflammation in Chronic Rhinosinusitis with Nasal Polyposis. *J. Asthma Allergy* **2021**, *14*, 585−593.

(31) Sim, H.; Jeong, D.; Kim, H. I.; Pak, S.; Thapa, B.; Kwon, H. J.; Lee, K. CD11b Deficiency Exacerbates Methicillin-Resistant Staphylococcus aureus-Induced Sepsis by Upregulating Inflammatory Responses of Macrophages. *Immune Netw.* **2021**, *21* (2), e13.

(32) Maiti, A. K.; Kim-Howard, X.; Motghare, P.; Pradhan, V.; Chua, K. H.; Sun, C.; Arango-Guerrero, M. T.; Ghosh, K.; Niewold, T. B.; Harley, J. B.; Anaya, J. M.; Looger, L. L.; Nath, S. K. Combined protein- and nucleic acid-level effects of rs1143679 (R77H), a lupus-predisposing variant within ITGAM. *Human molecular genetics* **2014**, *23* (15), 4161−76.

(33) Botero, J. P.; Lee, K.; Branchford, B. R.; Bray, P. F.; Freson, K.; Lambert, M. P.; Luo, M.; Mohan, S.; Ross, J. E.; Bergmeier, W.; Di Paola, J. Glanzmann thrombasthenia: genetic basis and clinical correlates. *Haematologica* **2020**, *105* (4), 888−894.

(34) Dumon, S.; Walton, D. S.; Volpe, G.; Wilson, N.; Dassé, E.; Del Pozzo, W.; Landry, J. R.; Turner, B.; O'Neill, L. P.; Göttgens, B.; Frampton, J. Itga2b regulation at the onset of definitive hematopoiesis and commitment to differentiation. *PLoS One* **2012**, *7* (8), e43300.

(35) Zhao, M.; Rabieifar, P.; Costa, T. D. F.; Zhuang, T.; Minden, A.; Lohr, M.; Heuchel, R.; Stromblad, S. Pdx1-Cre-driven conditional gene depletion suggests PAK4 as dispensable for mouse pancreas development. *Sci. Rep.* **2017**, *7* (1), 7031.

(36) Hu, Q.; Lyon, C. J.; Fletcher, J. K.; Tang, W.; Wan, M.; Hu, T. Y. Extracellular vesicle activities regulating macrophage- and tissue-mediated injury and repair responses. *Acta Pharm. Sin B* **2021**, *11* (6), 1493−1512.

(37) Barczyk, M.; Carracedo, S.; Gullberg, D. Integrins. *Cell Tissue Res.* **2010**, *339* (1), 269−80.

(38) Sun, Z.; Guo, S. S.; Fässler, R. Integrin-mediated mechanotransduction. *J. Cell Biol.* **2016**, *215* (4), 445−456.

(39) Jiménez-Alesanco, A.; Marcuello, M.; Pastor-Jiménez, M.; López-Puerto, L.; Bonjoch, L.; Gironella, M.; Carrascal, M.; Abian, J.; de-Madaria, E.; Closa, D. Acute pancreatitis promotes the generation of two different exosome populations. *Sci. Rep.* **2019**, *9* (1), 19887.

(40) Wang, P.; Luo, R.; Zhang, M.; Wang, Y.; Song, T.; Tao, T.; Li, Z.; Jin, L.; Zheng, H.; Chen, W.; Zhao, M.; Zheng, Y.; Qin, J. A cross-talk between epithelium and endothelium mediates human alveolar-capillary injury during SARS-CoV-2 infection. *Cell Death Dis.* **2020**, *11* (12), 1042.

(41) Hu, Q.; Yao, J.; Wu, X.; Li, J.; Li, G.; Tang, W.; Liu, J.; Wan, M. Emodin attenuates severe acute pancreatitis-associated acute lung injury by suppressing pancreatic exosome-mediated alveolar macrophage activation. *Acta Pharm. Sin B* **2022**, *12* (10), 3986−4003.

(42) Choi, H.; Choi, Y.; Yim, H. Y.; Mirzaaghasi, A.; Yoo, J. K.; Choi, C. Biodistribution of Exosomes and Engineering Strategies for Targeted Delivery of Therapeutic Exosomes. *Tissue engineering and regenerative medicine* **2021**, *18* (4), 499−511.

(43) Liu, Y.; Cao, X. Organotropic metastasis: role of tumor exosomes. *Cell Res.* **2016**, *26* (2), 149−50.

(44) Li, Z.; Wang, Z.; Dinh, P. C.; Zhu, D.; Popowski, K. D.; Lutz, H.; Hu, S.; Lewis, M. G.; Cook, A.; Andersen, H.; Greenhouse, J.; Pessaint, L.; Lobo, L. J.; Cheng, K. Cell-mimicking nanodecoys neutralize SARS-CoV-2 and mitigate lung injury in a non-human primate model of COVID-19. *Nat. Nanotechnol* **2021**, *16* (8), 942−951.

(45) Zhang, J.; Huang, F.; Xia, B.; Yuan, Y.; Yu, F.; Wang, G.; Chen, Q.; Wang, Q.; Li, Y.; Li, R.; Song, Z.; Pan, T.; Chen, J.; Lu, G.; Zhang, H. The interferon-stimulated exosomal hACE2 potently inhibits SARS-CoV-2 replication through competitively blocking the virus entry. *Sig. Transduct. Target Ther.* **2021**, *6* (1), 189.

(46) Jerke, U.; Rolle, S.; Purfürst, B.; Luft, F. C.; Nauseef, W. M.; Kettritz, R. β2 integrin-mediated cell-cell contact transfers active myeloperoxidase from neutrophils to endothelial cells. *J. Biol. Chem.* **2013**, *288* (18), 12910−9.

(47) Zhou, M.; Wang, X.; Shi, Y.; Ding, Y.; Li, X.; Xie, T.; Shi, Z.; Fu, W. Deficiency of ITGAM Attenuates Experimental Abdominal Aortic Aneurysm in Mice. *J. Am. Heart Assoc.* **2021**, *10* (7), e019900.

(48) Ge, P.; Luo, Y.; Okoye, C. S.; Chen, H.; Liu, J.; Zhang, G.; Xu, C.; Chen, H. Intestinal barrier damage, systemic inflammatory response syndrome, and acute lung injury: A troublesome trio for acute pancreatitis. *Biomed. Pharmacother.* **2020**, *132*, 110770.

(49) Hiroshima, Y.; Hsu, K.; Tedla, N.; Wong, S. W.; Chow, S.; Kawaguchi, N.; Geczy, C. L. S100A8/A9 and S100A9 reduce acute lung injury. *Immunology and cell biology* **2017**, *95* (5), 461−472.

(50) Carrascal, M.; Areny-Balagueró, A.; de-Madaria, E.; Cárdenas-Jaén, K.; García-Rayado, G.; Rivera, R.; Martin Mateos, R. M.; Pascual-Moreno, I.; Gironella, M.; Abian, J.; Closa, D. Inflammatory capacity of exosomes released in the early stages of acute pancreatitis predicts the severity of the disease. *Journal of pathology* **2022**, *256* (1), 83−92.

(51) Ding, Z.; Du, F.; Averitt, V. R.; Jakobsson, G.; Rönnow, C. F.; Rahman, M.; Schiopu, A.; Thorlacius, H. Targeting S100A9 Reduces Neutrophil Recruitment, Inflammation and Lung Damage in Abdominal Sepsis. *Int. J. Mol. Sci.* **2021**, *22* (23), 12923.

(52) Zhu, X.; Badawi, M.; Pomeroy, S.; Sutaria, D. S.; Xie, Z.; Baek, A.; Jiang, J.; Elgamal, O. A.; Mo, X.; Perle, K.; Chalmers, J.; Schmittgen, T. D.; Phelps, M. A. Comprehensive toxicity and immunogenicity studies reveal minimal effects in mice following sustained dosing of extracellular vesicles derived from HEK293T cells. *Journal of extracellular vesicles* **2017**, *6* (1), 1324730.